Proceedings of the 18th Iranian Geophysical Conference, May 2018, pages 68-71

Seismotectonic characteristics of the 2017 Sefid Sang (Mw 6) earthquake

Aflaki, M.[1], Ghods, A.[2], Mousavi, Z.[1], Shabanian, E.[1], Vajedian, S.[3] and Akbarzadeh, M.[4]

[1]*Assistant professor, Department of Earth Sciences, Institute for Advanced Studies in Basic Sciences, Zanjan, Iran, aflaki@iasbs.ac.ir, z.mousavi@iasbs.ac.ir, shabanian@iasbs.ac.ir*

[2]*Associate professor, Department of Earth Sciences, Institute for Advanced Studies in Basic Sciences, Zanjan, Iran, aghods@iasbs.ac.ir*

[3]*Institute of Photogrammetry and GeoInformation (IPI), Leibniz Universität Hannover, Germany, vajedian@ipi.uni-hannover.de*

[4]*PhD student, Department of Earth Sciences, Institute for Advanced Studies in Basic Sciences, Zanjan, Iran, m.akbarzadeh@iasbs.ac.ir*

ABSTRACT

The 5th April 2017 Sefid Sang earthquake rise an opportunity to study the deformation pattern in the SE of the Kopeh Dagh Mountains. Multiple event relocation of the Sefid Sang main shock and its 59 aftershocks shows unidirectional rupture directivity from NW to SE. The focal mechanisms for the mainshock and the two largest aftershocks reveal a mainly reverse mechanism (with average strikes of ~300 and ~70 for fault planes) with a small strike-slip component. The optimal model based on InSAR data indicates a NE- dipping reverse fault, which is consistent with the NE-dipping fault plane of the focal mechanism and the aftershock pattern. To characterize the regional stress state, we performed an extensive field measurement of fault kinematics in the study area. Separate inversion of both geological and seismological fault slip data indicates a similar transpressional stress regime (NNE-oriented compression) for the study area. These results indicate the change in the kinematics of deformation from strike-slip faulting along the main NNW-striking faults (e.g., Bakharden-Quchan fault system) to reverse faulting at their WNW-striking terminations (e.g., Neyshabur fault and southern termination of the Hezar Masjed fault systems).

Keywords: Sefid Sang earthquake, Seismology, InSAR, slip distribution, stress inversion, Focal mechanism.

INTRODUCTION

The Kopeh Dagh Mountains in NE of Iran experienced several destructive events (M~6.5-7.5), most of them were concentrated along the major deep-seated Main Kopeh Dagh, Bakharden-Quchan and Neyshabur fault systems. Within the Kopeh Dagh and Binalud ranges, most of ongoing deformation is accumulating by transpressional faulting (e.g., along NW-striking Neyshabur fault system), as deduced from both geodetic (Mousavi et al., 2013) and geologic (e.g., Shabanian et al., 2009) data. Also, the NNW-striking Bakharden-Quchan fault system is transferring deformation towards NW by strike-slip faulting (e.g., Shabanian et al., 2012). The NW-striking faults, like Hezar Masjed and Kashafrud fault systems show different structural and kinematic characteristics (Shabanian et al., 2010). The 5th April 2017 Sefid Sang event occurred at the southern termination of Hezar Masjed fault system near the town of Fariman. This provides us an excellent opportunity to investigate the pattern of strain accommodation in the southern termination of the Kopeh Dagh range. We present a multi-disciplinary research based on integrated geological, seismological and InSAR data complemented by the inversion of fault kinematics.

METHODOLOGY AND DATA

Seismology

We have located the Sefid Sang mainshock (6 Mw) and its 115 aftershocks by single event location (using SEISAN software; Havskov & Otemoller 1999) and multiple event relocation based on the Hypocentroidal Decomposition (HD) algorithm (Jordan & Sverdrup, 1981) (Fig. 1a). We use data from permanent seismic stations of IRSC (Iranian Seismological Center), EQRC (Earthquake Research Center of Ferdowsi University of Mashhad), INSN (Iranian National Seismograph Network) and IRIS (Incorporated Research Institutions for Seismology) networks. Differential times of Sg–Pg phases were picked from BHRC (Building and Housing Research Center) network of digital accelerometers for the two larger events in the cluster. The BHRC stations in the study area do not have calibrated GPS timing, so we utilize differential phase readings.

In single event location, we have only used Pg and Sg phases to avoid the large travel time error of Pn phases. The Pn phases along with other regional and teleseismic phases reported by International Seismic Center (ISC) were used in the multiple event relocation method to improve the relative relocation of the events. To form the Sefid Sang cluster, 59 well located events have been selected. The location of Sefid Sang mainshock relative to its aftershocks indicates almost unidirectional rupture directivity from NW to SE. The length of aftershock zone is about 24 km, considerably larger than what is expected for a 6.0 Mw event.

We also estimated precisely the focal depths of 53 events out of the 59 events in the cluster, including the mainshock with focal depth of 15 km. Furthermore, the first arrival focal mechanisms for the mainshock and the

two larger aftershocks have been determined using 48 local and regional polarities covering all the four quadrants (Fig. 1b). The results show mainly reverse mechanisms with small dextral strike-slip component.

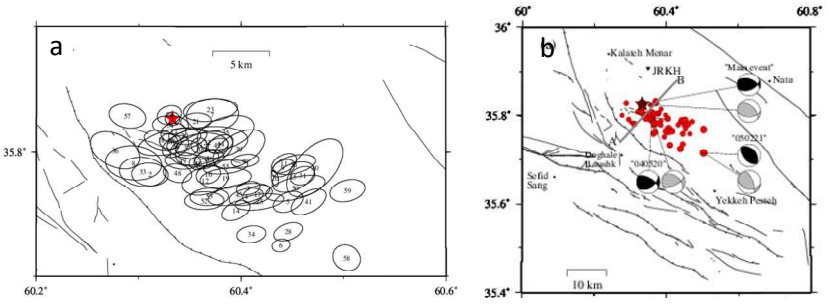

Fig.1:a) Relocation of 59 events of Sefid Sang cluster, using the multiple-event relocation method. The 90 percent confidence ellipses for the relative locations of epicenters are shown. The mainshock is highlighted by a red star. b) The epicenter of 53 relocated events of Sefid Sang cluster (the red circles). The black and grey beach balls shows the focal mechanisms determined in this study and those of double couple part component of CMT Global solutions, respectively.

InSAR

We investigate the areal extent of ground deformation due to the Sefid Sang earthquake using Interferometric Synthetic Aperture Radar (InSAR) measurements. The affected area by earthquake was covered by one descending and ascending tracks of the S1 TOPS C-band SAR imagery. We produced 12 days interferograms from SLC (Single Look Complex) products using GMTSAR Package (Sandwell et al., 2016). The resultant ascending and descending interferograms reveals surface displacement on hanging wall with maximum 12 cm toward the satellite (Fig.2a&b). We inverted the unwrapped interferograms using Okada's (1985) Green functions to obtain fault parameters, assuming a single rectangular plane in a uniform half space. The inverted fault geometry parameters are location, size and orientation of the fault plane. The optimal resultant parameters indicate a northeast dipping reverse fault with dip of 38° and fault length of 11 km.

In the second step, we fixed the parameters of strike, dip, rake and location of the fault plane to those derived from the uniform slip solution, and inverted the InSAR coseismic displacement map to estimate slip variations on the fault plane. We extended the fault along strike 20 km and along down dip to the depth of 16 km. The fault plane was subdivided into an array of rectangular 800 m along strike by 640 m along dip, a total of 25 by 25 patches on the fault plane. Figure 2c shows the resultant fault slip distribution with peak slip of 70 cm occurred at a depth of 8 km on central part of the fault plane. Considering 30 GPa for rigidity modulus, we estimated seismic moment equal to 2.681e+18Nm for optimal solution equivalent to a moment magnitude of 6.2, slightly (0.2 unit) larger than the CMT solution.

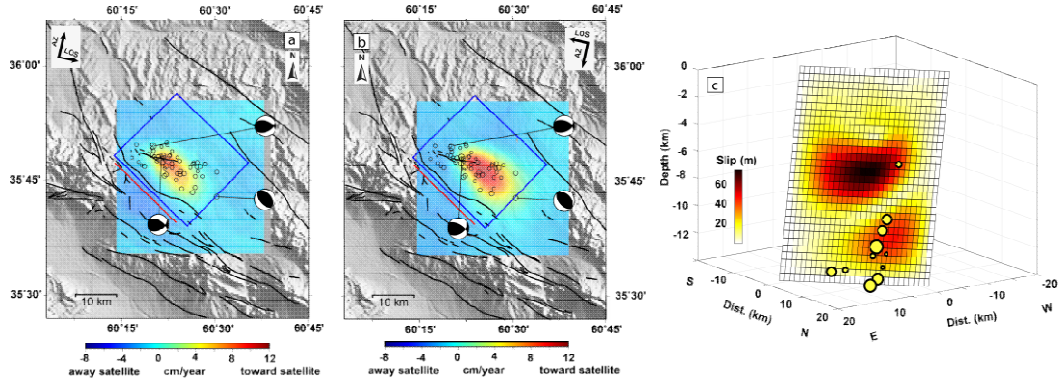

Fig.2: Ground surface deformation from InSAR for ascending (a) and descending (b) track superposed on a shaded-relief DEM (SRTM). Black lines and circles are fault traces and aftershocks locations, respectively. The black beach balls shows the focal mechanisms determined in this study. The causative fault of the main shock, obtained from uniform slip inversion, is shown in red. The blue rectangle presents the modeled fault plane. c) Slip distribution obtained from linear inversion with variable slip. The yellow circles show the location of aftershocks obtained from seismologic data.

Active state of stress deduced from geological and seismological data

The active stress state in the area of interest was determined through the inversion of fault-slip data measured in the field and obtained from focal mechanisms of earthquakes. We measured the geological fault-slip data in 11 sites on striated fault planes cutting Quaternary, Plio-Quaternary and Pre-Neogene unites, as well as on faces of striated carbonate pebbles of Neogene conglomerates.

Inhomogeneous fault-slip data collected in each site are chronologically sorted to distinct homogenous data sets using usual cross-cutting and relative chronologic criteria for data separation. The inversion method inverted by Carey and Brunier (1974) and Carey (1979) is applied on the youngest data sets from six sites to determine modern stress state (Fig.3a) which is characterized by transpressional stress regime, with a N029°E-oriented horizontal compression (Fig. 3b).

The present-day stress state is obtained from the focal mechanism data of 13 individual earthquakes that occurred in the area of interest (Table 1) since 1970 and were collected from CMT (Shabanian et al. 2010) and this study (Sefid Sang mainshock and its two aftershocks). The focal mechanism data were analyzed using the principles proposed by Carey-Gailhardis and Mercier (1987). As the main step, the NW-striking nodal plane of the focal mechanism calculated for the Sefid Sang main shock is defined as the fault plane based on the distribution of aftershocks and InSAR co-seismic displacement map. This fault plane (azimuth/dip/rake in right-hand rule: 292/50/057) are used as a key data during the inversion process. Inversion result (Fig. 3c) represents an active compressional stress regime characterized by a N026E-oriented maximum horizontal stress dominated within the north eastern part of Iran, including the area of interest.

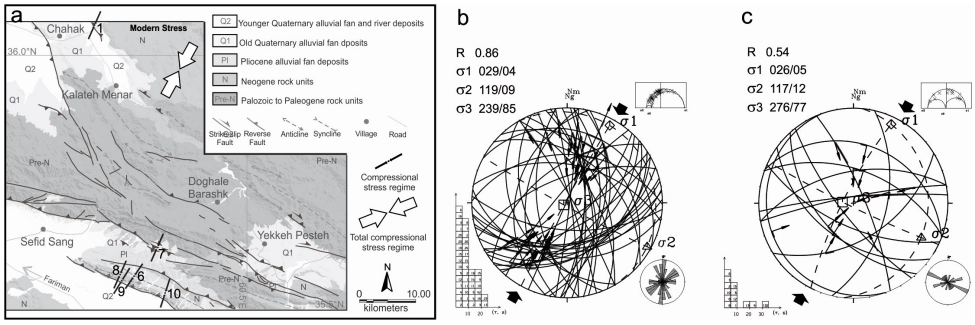

Fig.3: a) Simplified geological map of the study area, presents uniform NW-striking fold and reverse faults developed in Neogene to older Paleozoic rock units. Thick black lines present the direction of maximum horizontal stresses for the modern compressional stress regime b) Lower hemisphere stereographic projections of fault slip data measured in 11 sites and the components of regional modern state of stress. c) Lower hemisphere stereographic projections revealing the active state of stress resulted from the inversion of earthquake focal mechanisms.

CONCLUSIONS

Both CMT and first polarity solutions show a mostly reverse mechanism with small dextral strike-slip component for the mainshock and the two aftershocks. These data are consistent with the result of InSAR slip distribution modeling and the kinematic analysis of geological faults measured in the field. The coinciding results of the inversion of both geologically- and seismologically-derived fault-slip data reveal the earthquake fault reactivation in a uniform regional transpressional stress state. Our original results indicate that strike-slip faulting along the NNW-striking faults through the Kopeh Dagh Mountains is transferred southeast and is changed into dominantly reverse kinematics at their WNW-striking terminations. This compressional kinematics on WNW-striking faults is a common feature for accommodating N-S dextral shear between the southern termination of the Kopeh Dagh-Binalud faults and the eastern termination of the Doruneh fault system.

Table1:A) Earthquake parameters including focal mechanism data used in the inversion method. B) The present-day stress obtained from the inversion of focal mechanism data.

a) Earthquake source parameters													
Site	Date	Time	Lat.	Long.	Mb/Mw	Plane 1			Plane 2			Depth	Refrence
No.	(yyyymmdd)	(hhmm)	(°N)	(°E)		Azimuth	Dip	Rake	Azimuth	Dip	Rake	(Km)	
1	19700101	1431	37.32	59.6	5.0/-	291	26	97	103	64	87	23	Shabanian et al., 2010
2	19700404	1058	36.99	59.47	4.9/-	73	68	15	337	76	157	_	Shabanian et al., 2010
3	19770809	2142	36.74	60.13	4.6/-	243	57	19	142	74	145	8	Shabanian et al., 2010
4	19850816	1047	36.96	59.72	-/5.6	265	82	65	159	26	162	10	CMT cataloge
5	19921127	2109	37.36	59.77	-/5.3	166	68	172	259	82	22	24	CMT cataloge
6	19991108	2137	36.04	61.38	-/5.5	304	43	88	126	47	92	44.5	CMT cataloge
7	19991109	521	35.78	61.29	-/5.3	160	5	89	342	85	90	24.9	CMT cataloge
8	19991109	1149	35.9	61.19	-/4.9	162	43	67	13	51	110	22.8	CMT cataloge
9	19991205	1312	35.91	61.5	-/4.9	107	41	112	259	53	72	20	CMT cataloge
10	20030703	1459	35.66	60.84	-/5.1	316	30	109	114	62	79	30	CMT cataloge
11	20170405	609	35.81	60.37	-/6.0	312	53	117	91	44	59	12	CMT cataloge
			35.83	60.33	-	292	50	57	66	50	57	15	This study
12	20170405	2007	35.84	60.4	-/5.0	307	47	143	64	64	50	16.7	CMT cataloge
			35.81	60.36	-	300	62	131	58	48	39	18	This study
13	20170502	2112	35.66	60.58	-/5.1	102	39	43	336	64	121	12	CMT cataloge
			35.72	60.5	-	138	50	90	318	40	90	~16?	This study

b) Resulted deviatoric stress tensors									
Zone	61		62		63		R	N	Rm
	Trend	Plunge	Trend	Plunge	Trend	Plunge			
	26	5	117	12	276	77	0.54	13	C

REFERENCES

Carey, E. 1979. Recherche des directions principales de contraintes associe´es au jeu d'une population de failles, Rev. Geol. Dyn. Geogr. Phys., 21, 57 – 66, http://worldcat.org/issn/00351164

Carey, E., and Brunier B., 1974.Analyse the´orique et nume´rique d'un mode`le me´canique e´le´mentaire applique´a` l'e´tude d'une population de failles, C. R. Acad. Sci., Ser. D, 279, 891 – 894, Doi:10012030845

Carey-Gailhardis, E., Mercier, J.-L., 1987. A numerical method for determining the state of stress using focal mechanism of earthquake populations: application to Tibetan teleseisms and microseismicity of southern Peru. Earth Planet. Sci. Lett. 82, 165–179, https://doi.org/10.1016/0012-821X(87)90117-8

Havskov, J. and Ottemoller, L., 1999. SEISAN: The Earthquake Analysis Software, version 8.0, Institute of Solid Earth Physics, University of Bergen.

Jordan, T.H. & Sverdrup, K.A., 1981. Teleseismic location techniques and their application to earthquake clusters in the south-central Pacific, Bull. Seism. Soc. Am., 71, 1105–1130.

Mousavi, Z., Walpersdorf, A., Walker, R.T., Tavakoli, F., Pathier, E., Nankali, H.R.E.A., Nilfouroushan, F. and Djamour, Y., 2013. Global Positioning System constraints on the active tectonics of NE Iran and the South Caspian region. Earth and Planetary Science Letters, 377, pp.287-298,https://doi.org/10.1016/j.epsl.2013.07.007

Okada, Y., 1985. Surface deformation due to shear and tensile faults in a half-space. Bulletin of the seismological society of America, 75(4), pp.1135-1154.

Sandwell, D., Mellors, R., Tong, X., Xu, X., Wei, M., Wessel, P., 2016. GMTSAR: An InSAR Processing System Based on Generic Mapping Tools (2nd ed.). Technical Report. Scripps Institution of Oceanography, UC San Diego.

Shabanian, E., Bellier, O., Siame, L., Arnaud, N., Abbassi, M. R., and Cochemé,J. J., 2009. New tectonic configuration in NE Iran: Active strike-slip faulting between the Kopeh Dagh and Binalud mountains, Tectonics, 28, TC5002, Doi:10.1029/2008TC002444

Shabanian, E., Bellier, O., Abbassi, M. R., Siame, L. L., and Farbod, Y., 2010. Plio-Quaternary stress states in NE Iran: Kopeh Dagh and Allah Dagh-Binalud mountains, Tectonophysics, 480, 280–304, Doi:10.1016/ j.tecto.2009.10.022

Shabanian, E., Bellier, O., Siame, L., Abbassi, M.R., Bourlès, D., Braucher, R. and Farbod, Y., 2012. The Binalud Mountains: A key piece for the geodynamic puzzle of NE Iran. Tectonics, 31(6),Doi: 10.1029/2012TC003183